Noise-Suppressing Newton Algorithm for Kinematic Control of Robots

Xiuchun Xiao, Lin Wei, Dongyang Fu, Jingwen Yan, Huan Wang

***Abstract*—In this paper, armed with the integral control method, a new noise-suppressing Newton (NSN) algorithm is proposed for the redundancy resolution of redundant robot manipulators efficiently. For practical hardware implementation, the discrete-time noise-suppressing Newton (abbreviated as DTNSN) algorithm is discretized from the continues NSN algorithm. Specifically, the distinguishing feature of the proposed DTNSN algorithm is that it can rigorously converge with inherent tolerance to noises induced by communication jamming and computational systematical errors. In contrast, considerable traditional algorithms often dispose of noises with the high-degree filter from the viewpoint of signal processing, which requires a complex system structure and further results in a heavy computational burden. Note that theoretical analyses are provided to elaborate the convergent property of the DTNSN algorithm polluted with constant bias, time-dependent linear noises and bounded random noises. Besides, by the proposed DTNSN algorithm, the end effector of both serial and parallel redundant robot manipulators complete the allocated motion planning and are impervious to the noisy simulated environment.**

***Index Terms*—Noise-suppressing Newton algorithm, the redundancy resolution, serial redundant robot manipulators, parallel redundant robot manipulators.**

I. Introduction

THERE exists a superior branch of robot arms referred to as redundant robot manipulators whose degrees of freedom (DOF) are more than that an end effector needs to conduct the allocated primary task [1]. Owing to the advanced performance, redundant robot manipulators are widely applied in various fields such as industry, medical engineering, etc [2]–[4].

This work was supported in part by the National Natural Science Foundation of China under Grant 61703189, in part by the International Science and Technology Cooperation Program of China under Grant 2017YFE0118900, in part by the Key Laboratory of Digital Signal and Image Processing of Guangdong Province under Grant 2016GDDSIPL-02, in part by the Doctoral Initiating Project of Guangdong Ocean University under Grant E13428, in part by the Innovation and Strength Project of Guangdong Ocean University under Grant Q15090 and Grant 230419065, in part by the Natural Science Foundation of Gansu Province, China, under Grant 18JR3RA264, in part by the Sichuan Science and Technology Program under Grant 19YYJC1656, in part by the State Key Laboratory of Management and Control for Complex Systems, Institute of Automation, Chinese Academy of Sciences under Grant 20190112, and in part by the Fundamental Research Funds for the Central Universities under Grant lzujbky-2019-89. (Corresponding authors: Dongyang Fu and Jingwen Yan).

X. Xiao, D. Fu and H. Wang are with the College of Electronic and Information Engineering, Guangdong Ocean University, Zhanjiang, 524088, China (e-mail: xcxiao@hotmail.com; fdy163@163.com).

L. Wei is with the School of Information Science and Engineering, Lanzhou University, Lanzhou 730000, China.

J. Yan is with the College of Electronic Engineering, Shantou University, Shantou, 515000, China (e-mail: Jwyan@stu.edu.cn).

Generally, it is difficult to construct redundancy resolution schemes on the joint angle since the kinematics equation is strongly nonlinear [1], [5]. Thereby, finding the solution to the redundancy resolution problem with the joint velocity being the independent variable is a classic and functional method [2], [3], [6]. The research [7] provides a method on account of the recurrent neural network for solving the velocity-level redundancy resolution problem, which also deals with joint acceleration limits effectively. In the previous research of redundancy resolution, the pseudoinverse-type method has been applied to redundant manipulators, which online calculates the pseudoinverse of the Jacobian matrix related to the kinematics formulation [8], [9]. In addition, a broad variety of algorithms, for example, adaptive learning control and its extensions are adept to realize the motion planning of redundant manipulators [10]–[19].

However, previous studies of the redundancy resolution have not treated the affect of noises caused by hardware facilities and/or human improper operations in detail [20]. For most conventional schemes, it is inevitable to design the filter which further requires other modules to monitor and measure the frequency, amplitude or other parameters of noises, so as to confront the interference. Nevertheless, the interplay among the filters, monitoring modules and the scheme for redundancy resolution, would prevent the overall redundant manipulator from maintaining stable in all likelihood [21]. Generally speaking, all the previously mentioned limitations and the resultant complex structure impede extensive applications of existing conventional algorithms in redundant manipulators.

Newton-Raphson iterative is effective for root-finding, which generates successively better approximations to the roots of a real-valued function, but could not produces accurate solutions in noisy workspace because of the inability to cope with external and internal unknown noises [22]. In consequence, inspired by the integral control, the noise-suppressing Newton (NSN) algorithm is proposed and investigated in this paper. With inherent denoisy capacity, the NSN algorithm rapidly converges to the analytical solution to the redundancy resolution of redundant manipulators in the presence of noises.

The remaining part of the paper is arranged into five sections. The discrete-time NSN algorithm is proposed to solve the redundant resolution in Section II. Besides, extended solutions to the discrete-time NSN algorithm in serial and parallel redundant manipulators are provided in Section III with the comparable existing methods. Section IV presents the theoretical analyses on how discrete-time NSN algorithm converges with various kinds of noises. In Section V, illustrative simulation examples related to manipulator motion planning

are provided for verifying the correctness and superiority of the proposed discrete-time NSN algorithm for redundant manipulators. In the end, section VI concludes the paper.

The main contributions made by this paper are pointed out as below.

1) By the powerful and succinct structure, the NSN algorithm is not only well-designed to find the ideal solution to redundant resolution problems but robust to noises and disturbances.
2) The NSN algorithm provides insight for extending the Newton-Raphson iteration from the classic computation viewpoint to the integral control viewpoint.
3) Theoretical analyses on how the NSN algorithm converges with constant bias, time-dependent linear noises and bounded random noises guarantee its stability and efficiency.
4) Synthesized by the newly proposed NSN algorithm, the experimental simulation of anti-noise manipulator motion planning is smoothly and precisely carried out in serial and parallel redundant manipulators.

II. Problem Formulation and Algorithm Design

The section below briefly presents the problem formulation and methodically proposes the NSN algorithm.

A. Redundant Manipulator Kinematics

For background knowledge, the forward kinematics of redundant robot manipulators is necessary to clarify here. Given that time t_k is sampled by gap l as $t = (k+1)l, k \in \mathbb{N}$, that $\theta(t_k) \in \mathbb{R}^m$ represents joint angle vector sampled at kth time instant, and that the running time of the end effector ranges from the start t_s to the end t_o with $[t_k, t_{k+1}) \subseteq [t_s, t_o]$, the forward kinematics is given here [23]:

$$\boldsymbol{\gamma}^{\mathrm{a}}(t_k) = g(\theta_k), \tag{1}$$

where the actual Cartesian coordinate of the end effector at t_k is represented by $\boldsymbol{\gamma}^{\mathrm{a}}(t_k) \in \mathbb{R}^n$; considering the Denavit-Hartenberg (D-H) convention [24], $g(\cdot) : \mathbb{R}^m \to \mathbb{R}^n$, is a continuous nonlinear function mapping from joint-angle space to the corresponding workspace. In addition, the dimension of $\boldsymbol{\gamma}^{\mathrm{a}}(t)$ is less than that of joint angle $\theta(t)$ $(n < m)$ for the manipulator is redundant.

In terms of redundancy resolution, the kinematic error-evolving equation is described as follow:

$$\boldsymbol{\varepsilon}(t_k) = \boldsymbol{\gamma}^{\mathrm{a}}(t_k) - \boldsymbol{\gamma}^{\mathrm{d}}(t_k), \tag{2}$$

where superscript $^{\mathrm{d}}$ on $\boldsymbol{\gamma}$ denotes the desired Cartesian coordinate of the end effector.

B. NSN Algorithm Design

To decrease the deviation between $\boldsymbol{\gamma}^{\mathrm{a}}(t_k)$ and $\boldsymbol{\gamma}^{\mathrm{d}}(t_k)$ with the presence of noises and further realize the redundancy resolution, a general equation as below is defined for discussion,

$$\min_{\mathbf{y}(t_k)\in\mathbb{R}^m} \varphi\big(\mathbf{y}(t_k)\big) \in \mathbb{R}^n. \tag{3}$$

Use $\varepsilon_n(t_k)$ to represent the nth element and subsequently $\boldsymbol{\varepsilon}(t_k) = [\varepsilon_1(t_k), \varepsilon_2(t_k), \cdots, \varepsilon_n(t_k)]^{\mathrm{T}} = \varphi(\mathbf{y}(t_k))$.

The design of the proposed NSN algorithm is composed of two steps. Firstly, the proposed superior integral control is formulated as

$$\boldsymbol{\varepsilon}(t) = -\frac{\kappa}{\varsigma}\int_0^t \boldsymbol{\varepsilon}(\beta)\mathrm{d}\beta, \tag{4}$$

where step size $\kappa > 0$ and $\varsigma > 0$ determine the rate of convergence. Secondly, supposing that sampling gap $l \to 0$, the continuous-time Newton Raphson iteration (NRI)

$$\dot{\mathbf{y}}(t) = -\frac{1}{l}J^{\dagger}(\mathbf{y}(t))\varphi(\mathbf{y}(t)) \tag{5}$$

can be approximated from the NRI method [25], where $J(\mathbf{y}(t)) = \partial\varphi(\mathbf{y}(t))/\partial\mathbf{y}(t)^{\mathrm{T}} \in \mathbb{R}^{n\times m}$ is the Jacobian matrix [26], [27] with symbol † standing for the pseudo-inverse operation. As a result, combining (4) and (5), the proposed NSN algorithm with unknown noises disturbing is given in a continuous manner

$$J(\mathbf{y}(t))\dot{\mathbf{y}}(t) = -\varsigma\varphi(\mathbf{y}(t)) - \kappa\int_0^t \varphi(\mathbf{y}(\beta))\mathrm{d}\beta + \Xi(t), \tag{6}$$

where $\Xi(t)$ denotes the unknown noise induced by observation error, methodical error, rounding error, communication noises and their reciprocity. Ulteriorly, provided that $J(\mathbf{y}(t))$ exists the form of pseudo inverse, the continuous-time NSN algorithm (6) is converted into

$$\dot{\mathbf{y}}(t) = -J^{\dagger}(\mathbf{y}(t))\big(\varsigma\varphi(\mathbf{y}(t)) + \kappa\int_0^t \boldsymbol{\varphi}(\mathbf{x}(\beta))\mathrm{d}\beta + \Xi(t)\big). \tag{7}$$

To readily implement the above continuous-time NSN algorithm (7) by hardware, the discrete-time NSN, namely DTNSN algorithm, is derived through Taylor expansion [28]

$$\begin{aligned}\mathbf{y}(t_{k+1}) =& \mathbf{y}(t_k) - J^{\dagger}(\mathbf{y}(t_k))\big(a_1\varphi(\mathbf{y}(t_k)) + \\ & a_2\sum_{j=0}^{k}\varphi(\mathbf{y}(t_j))\big),\end{aligned} \tag{8}$$

where step size $a_1 = l\varsigma$ and $a_2 = l\kappa$. Note that noise $\Xi(t)$ is removed for stressing the structure of DTNSN algorithm (8). It is of importance to select step-size a_1 and a_2 appropriately, which largely affects the noise-suppressing performance of integral controller. In this sense, to obtain the desired NSN algorithm (8), we need to adjust the step-size parameters, often iteratively by "tuning".

III. NSN Algorithm for Redundancy Resolution

The section that follows further applies the DTNSN algorithm (8) to serial and parallel redundant manipulators. In addition, other comparable algorithms including NRI and a serial of zeroing dynamics with Euler and Taylor discretization which are referred to as the ZDE algorithm and ZDT algorithm, respectively are also presented.

After combining forward kinematics (1), error-evolving equation (2) and DTNSN algorithm (8), we get the analytical solution to redundancy resolution problem of serial manipula-

TABLE I: Kinematic solutions of comparable algorithms for serial and parallel redundant manipulators

Solution	Serial Formulation
NRIS	$\theta_{k+1} = -J^{\dagger}(\theta_k)\left(g(\theta_k) - \boldsymbol{\gamma}_k^{\mathrm{d}}\right) + \theta_k$
ZDES	$\theta_{k+1} = J^{\dagger}(\theta_k)\left(l\dot{\boldsymbol{\gamma}}_k^{\mathrm{d}} - a_2\left(g(\theta_k) - \boldsymbol{\gamma}_k^{\mathrm{d}}\right)\right) + \theta_k$
ZDTS	$\theta_{k+1} = J^{\dagger}(\theta_k)\left(l\dot{\boldsymbol{\gamma}}_k^{\mathrm{d}} - a_2\left(g(\theta_k) - \boldsymbol{\gamma}_k^{\mathrm{d}}\right)\right) + 3/2\theta_k - \theta_{k-1} + 1/2\theta_{k-2}$
—-	———————————————
Solution	Parallel Formulation
NRIP	$\mathbf{b}_{k+1} = -L(\mathbf{b}(t_k), E(t_k))\left(\boldsymbol{\gamma}_k^{\mathrm{a}} - \boldsymbol{\gamma}_k^{\mathrm{d}}\right) + \mathbf{b}_k$
ZDEP	$\mathbf{b}_{k+1} = L(\mathbf{b}(t_k), E(t_k))\left(l\dot{\boldsymbol{\gamma}}_k^{\mathrm{d}} - a_2\left(\boldsymbol{\gamma}_k^{\mathrm{a}} - \boldsymbol{\gamma}_k^{\mathrm{d}}\right)\right) + \mathbf{b}_k$
ZDTP	$\mathbf{b}_{k+1} = L(\mathbf{b}(t_k), E(t_k))\left(l\dot{\boldsymbol{\gamma}}_k^{\mathrm{d}} - a_2\left(\boldsymbol{\gamma}_k^{\mathrm{a}} - \boldsymbol{\gamma}_k^{\mathrm{d}}\right)\right) + 3/2\mathbf{b}_k - \mathbf{b}_{k-1} + 1/2\mathbf{b}_{k-2}$

tor

$$\theta_{k+1} = -J^{\dagger}(\theta_k)\big(a_1(g(\theta_k) - \boldsymbol{\gamma}_k^{\mathrm{d}}) + a_2\sum_{j=0}^{k}(g(\theta_j) - \boldsymbol{\gamma}_j^{\mathrm{d}})\big) + \theta_k. \tag{9}$$

Note that the above equation (9) is called DTNSNS solution for short.

One of the most typical parallel robot is Gough-Stewart platform [30], which contains six prismatic actuators. Firstly, as a paramount step, several variables are defined to build the kinematics equation of the parallel manipulator. Column vector $\mathbf{b}_k$ contains the length information of six legs at time instant k with b_k^1, b_k^2 ,b_k^3, b_k^4, b_k^5 and b_k^6 being elements. Further, we apply DTNSN algorithm (8) to the Gough-Stewart platform [30] and get

$$\mathbf{b}(t_{k+1}) = -L(\mathbf{b}(t_k), E(t_k))\big(a_1(\boldsymbol{\gamma}_k^{\mathrm{a}} - \boldsymbol{\gamma}_k^{\mathrm{d}}) + a_2\sum_{j=0}^{k}(\boldsymbol{\gamma}_j^{\mathrm{a}} - \boldsymbol{\gamma}_j^{\mathrm{d}})\big) + \mathbf{b}(t_k), \tag{10}$$

where matrix $L(\mathbf{b}(t_k), E(t_k)) \in \mathbb{R}^{6\times 3}$ is related to leg lengths $\mathbf{b}(t_k)$ and $E(t_k) = [\mathbf{e}_k^1, \mathbf{e}_k^2, \mathbf{e}_k^3, \mathbf{e}_k^4, \mathbf{e}_k^5, \mathbf{e}_k^6] \in \mathbb{R}^{3\times 6}$ which represents the vector of each link in direction from base to top. Note that the above equation (10) is called DTNSNP solution for short.

To validate how DTNSN algorithm (8) surpasses other algorithms for the redundancy resolution of redundant manipulators with unknown noises jamming, Table I presents the NRI algorithm, ZDE algorithm, and ZDT algorithm [30]–[33] for serial and parallel redundant manipulators.

IV. Theoretical Analyses and Results

In terms of certifying the convergence performance of the proposed DTNSN algorithm (8) with various kinds of noises, we give the following theorems.

Theorem 1: Under theoretically noiseless conditions, the steady-state residual error $\lim_{k\to\infty}\|\boldsymbol{\varepsilon}(t_k)\|_2$ synthesized by DTNSN algorithm (8) drops to $O(l^2)$, where vector $\mathbf{O}(l^2)$ is made up of element $O(l^2)$ and $\|\cdot\|_2$ denotes the Euclidean norm.

Proof: In the beginning, by simply transposing, DTNSN algorithm (8) transforms into

$$J(\mathbf{y}(t_k))(\mathbf{y}(t_{k+1}) - \mathbf{y}(t_k)) = -a_1\varphi(\mathbf{y}(t_k)) - a_2\sum_{j=0}^{k}\varphi(\mathbf{y}(t_j)) \tag{11}$$

which is obviously equal to

$$\begin{aligned} &J(\mathbf{y}(t_k))\big(\mathbf{y}(t_{k+1}) - \mathbf{y}(t_k)\big) + \big(\varphi(\mathbf{y}(t_k)) - \varphi(\mathbf{y}(t_{k-1}))\big) \\ &= -a_1\varphi(\mathbf{y}(t_k)) - a_2\sum_{j=0}^{k}\varphi(\mathbf{y}(t_j)) + \varphi(\mathbf{y}(t_k)) - \\ &\varphi(\mathbf{y}(t_{k-1})). \end{aligned} \tag{12}$$

Substituting Taylor expansion formula [30] into equation (12) obtains

$$\begin{aligned} &J(\mathbf{y}(t_k))l\dot{\mathbf{y}}(t_k) + l\dot{\varphi}(\mathbf{y}(t_k)) + \mathbf{O}(l^2) \\ &= -a_1\varphi(\mathbf{y}(t_k)) - a_2\sum_{j=0}^{k}\varphi(\mathbf{y}(t_j)) + \varphi(\mathbf{y}(t_k)) - \\ &\varphi(\mathbf{y}(t_{k-1})). \end{aligned} \tag{13}$$

Then, according to the principle of partial differential, the above equation (13) with regard to $\boldsymbol{\varepsilon}(t_k)$ is converted into

$$l\dot{\boldsymbol{\varepsilon}}(t_k) + \mathbf{O}(l^2) = -a_1\boldsymbol{\varepsilon}(t_k) - a_2\sum_{j=0}^{k}\boldsymbol{\varepsilon}(t_j) + \boldsymbol{\varepsilon}(t_k) - \boldsymbol{\varepsilon}(t_{k-1}). \tag{14}$$

Finally, discretizing $\dot{\varepsilon}(t_k)$ [30], we obtain

$$a_1\varepsilon(t_k) + a_2\sum_{j=0}^{k}\varepsilon(t_j) + \mathbf{O}(l^2) = 0. \tag{15}$$

Considering the ith subsystem of equation (15), one can readily educe

$$a_1\varepsilon^i(t_k) + a_2\sum_{j=0}^{k}\varepsilon^i(t_j) + O(l^2) = 0. \tag{16}$$

Next, the time difference equation of (16) is provided

$$(a_1 + a_2)\varepsilon^i(t_{k+1}) = a_1\varepsilon^i(t_k) + O(l^2). \tag{17}$$

In order to transform formula (17) into state-space representation, the definition $A^i(t_{k+1}) = [\varepsilon^i(t_{k+1}), \varepsilon^i(t_k)]^{\mathrm{T}}$ is given and then we can get

$$A^i(t_{k+1}) = \mathcal{G}A^i(t_k) + \mathbf{O}(l^2), \tag{18}$$

with $\mathcal{G} = [a_1/(a_1 + a_2), 0; 1, 0]$. Then, in accordance with Triangle Inequality, it is elicited

$$\begin{aligned}
\|A^i(t_{k+1})\|_2 &\leq \|\mathcal{G}A^i(t_k)\|_2 + \|\mathbf{O}(l^2)\|_2 \\
&\leq \|\mathcal{G}\|_2\|A^i(t_k)\|_2 + O(l^2) \\
&\leq \|\mathcal{G}\|_2\|\mathcal{G}A^i(t_{k-1})\|_2 + \|\mathcal{G}\|_2 O(l^2) + O(l^2) \\
&\leq \|\mathcal{G}\|_2^2\|A^i(t_{k-1})\|_2 + O(l^2) \\
&\vdots \\
&\leq \|\mathcal{G}\|_2^k\|A^i(t_1)\|_2 + O(l^2).
\end{aligned} \tag{19}$$

Given that the eigenvalues of $\mathcal{G}$ are $c_1 = a_1/(a_1 + a_2)$ and $c_2 = 0$, whose absolute values are both less than 1. Therefore, from (19), we can infer $\lim_{k\to\infty}\|\mathcal{G}\|_2^k = 0$ and subsequently

$$\lim_{k\to\infty}\|A^i(t_{k+1})\|_2 \leq \lim_{k\to\infty}\|\mathcal{G}\|_2^k\|A^i(t_1)\|_2 + O(l^2) = O(l^2). \tag{20}$$

Thus, the steady-state residual error of DTNSN algorithm (8) can drop to $O(l^2)$. The proof is thus completed. ■

Theorem 2: Under linear noise $\mathbf{\Xi}(t_k) = pt_k + s$, the steady-state residual error of DTNSN algorithm (8) is $\lim_{k\to\infty}\|\varepsilon(t_k)\|_2$ is $\|p/a_2\|_2 + O(l^2)$ which degrades to $O(l^2)$ when linear noises become constant bias as $p = 0$.

Proof: Let us discuss what role linear noises play in

$$a_1\varepsilon^i(t_k) = -a_2\sum_{j=0}^{k}\varepsilon(t_j) + p^i kl + s^i. \tag{21}$$

Conducting the Z-transformation on equation (21), it is presented as

$$\varepsilon^i(z) = \frac{p^i lz + s^i z(z-1)}{a_1(z-1)^2 + a_2 z(z-1)}, \tag{22}$$

where the poles of denominator are, $z_1 = 1$ and $z_2 = a_1/(a_1 + a_2)$. Subsequently, according to Z-transformation final theorem, the infinite limit of $\varepsilon^l(t_k)$ is

$$\begin{aligned}
&\lim_{k\to\infty}\varepsilon^i(t_k) = \lim_{z\to 1}(z-1)\varepsilon^i(z) \\
=\ &\lim_{z\to 1}\frac{p^i lz + s^i z(z-1)}{a_1(z-1) + a_2 z} \\
=\ &\frac{p^i l}{a_2}.
\end{aligned} \tag{23}$$

Consequently, the steady-state residual error of DTNSN algorithm (8) is generated from linear noises which is

$$\lim_{k\to\infty}\|\varepsilon(t_k)\|_2 = \|\frac{pl}{a_2}\|_2 = \frac{pl}{a_2}$$

and inherent algorithm itself which is $O(l^2)$.

In conclusion, the steady-state residual error of DTNSN algorithm (8) influenced by linear noises approaches to $pl/a_2 + O(l^2)$. If $p = 0$, linear noises fall into constant bias $\mathbf{\Xi}(t_k) = s$ and the steady-state residual error of DTNSN algorithm (8) under constant bias is obtained

$$\lim_{k\to\infty}\|\varepsilon(t_k)\|_2 = O(l^2).$$

The proof is thus completed. ■

In the subsequent part, the orientation is to investigate the effect of bounded random noises acting on the DTNSN algorithm (8).

Theorem 3: The steady-state residual error of DTNSN algorithm (8) with bounded random noise $\Xi(t) = \chi$ is $\lim_{k\to\infty}\|\varepsilon(t_k)\|_2 = 2m\ \sup_{1\leq f\leq k,\ 1\leq q\leq m}\ |l_f^q|/(1-\|\mathcal{G}\|_2) + O(l^2)$.

Proof: Likewise the superposition method conducted in Theorem 3, the residual error triggered by bounded random noises and other factors is allowed to be deduced individually. Consequently, the difference equation related to bounded random noise is

$$(a_1 + a_2)\varepsilon^i(t_{k+1}) = a_1\varepsilon^i(t_k) + \chi^i(t_k) - \chi^i(t_{k-1}). \tag{24}$$

Defining a matrix $\varrho^i(t_k) = [\chi^i(t_k) - \chi^i(t_{k-1}), 0]^{\mathrm{T}}$, thereby equationGough-Stewart (24) with regard to $A^i(t_k)$ could be

$$A^i(t_{k+1}) = \mathcal{G}A^i(t_k) + \varrho^i(t_k), \tag{25}$$

Afterwards, the two-norm of $A^i(t_{k+1})$ is estimated through applying Triangle Inequality, which is

$$\begin{aligned}
&\|A^i(t_{k+1})\|_2 \\
&\leq \|\mathcal{G}A^i(t_k)\|_2 + \|\varrho^i(t_k)\|_2 \\
&\leq \|\mathcal{G}\|_2\|A^i(t_k)\|_2 + \|\varrho^i(t_k)\|_2 \\
&\leq \|\mathcal{G}\|_2\|\mathcal{G}A^i(t_{k-1})\|_2 + \|\mathcal{G}\|_2\|\varrho^i(t_{k-1})\|_2 + \|\varrho^i(t_k)\|_2 \\
&\leq \|\mathcal{G}\|_2^2\|A^i(t_{k-1})\|_2 + \|\mathcal{G}\|_2\|\varrho^i(t_{k-1})\|_2 + \|\varrho^i(t_k)\|_2 \\
&\vdots \\
&\leq \|\mathcal{G}\|_2^k\|A^i(t_1)\|_2 + \|\mathcal{G}\|_2^{k-1}\|\varrho^i(t_1)\|_2 + \ldots + \|\varrho^i(t_k)\|_2 \\
&< \|\mathcal{G}\|_2^k\|A^i(t_1)\|_2 + \max_{1\leq f\leq k}\|\varrho_p^i\|_2/(1-\|\mathcal{G}\|_2) \\
&< \|\mathcal{G}\|_2^k\|A^i(t_1)\|_2 + 2\max_{1\leq f\leq k}|\chi_p^i|/(1-\|\mathcal{G}\|_2).
\end{aligned} \tag{26}$$

Due to the value range that $\|\mathcal{G}\|_2 < 1$, it is evident that

$\lim_{k\to\infty}\|\mathcal{G}\|_2^k = 0$ so as to ensure

$$\lim_{k\to\infty}\|A_{k+1}^l\|_2<2\max_{1\le f\le k}|\chi_p^i|/(1-\|\mathcal{G}\|_2).$$

In the end, superimposing the residual error of each subsystem, we can get

$$\lim_{k\to\infty}\|\boldsymbol{\varepsilon}(t_k)\|_2<2m\sup_{1\le f\le k,\ 1\le q\le m}|\chi_p^l|/(1-\|\mathcal{G}\|_2)+O(l^2).$$

The proof is completed. ■

V. Simulative Experiments

In this section, simulative experiments are conducted to validate the extraordinary performance of the proposed DTNSN algorithm (8) for the redundancy resolution based on serial and parallel redundant manipulators, compared with other algorithms listing in Table I.

A kinematic "butterfly" motion planning task for the serial redundant manipulator is allocated as

$$\boldsymbol{\gamma}^{\mathrm{d}}(t_k) = e^{\cos(\theta_k)} - 2\cos(4\theta_k) + \sin^5(\theta_k/12), \tag{27}$$

where the whole running time and the initial value of $\theta_k \in \mathbb{R}^5$ is set to be 10 s and $\theta_0 = [0, -\pi/6, \pi/2, -\pi/4, 0]^{\mathrm{T}}$, respectively. In this example, the steady-state residual error $\|\boldsymbol{\varepsilon}(t_k)\|_2$ is chosen as the main indicator measuring whether DTNSNS solution (9) and other existing solutions listed in Table I are capable of withstanding unknown noises for the illustrative redundancy resolution problem (27).

Fig. 1 and Fig. 2 plot the comparable results that DTNSN solution (9) and other existing traditional algorithms (Table I) generate for "butterfly" motion planning (27) under the constant bias disturbing, from the perspective of the end-effector trajectory of the serial manipulator, joint angle and the residual error, respectively. As shown in Fig. 1, under constant bias $\Xi(t) = 2$, the steady-state residual error of DTNSNS solution (9) is as low as 10^{-6}, which leads to the actual path of the end effector consistently coinciding with the desired "butterfly" path. Besides, what plots in Fig. 1(c) illustrates that the end effector of the serial manipulator rotates within the normal working range. In contrast, as Fig. 2 plots, the actual path of the end effector implanted by NRIS solution (Table I) completely diverges from the desired path, where the steady-state residual error of NRIS solution (Table I) is almost 10 meters as well as ZDES solution and ZDTS solution (Table I).

Note that for the parallel manipulator, it is vividly shown in Fig. 3(a) and Fig. 3(b) that the trajectory of the end effector generated by DTNSNP solution (10) is the same as the actual path with the presence of noises. However, as seen in Fig. 3(c), NRIP solution (Table I) fails to complete the given motion planning task (28).

For the parallel redundant manipulator, a six-DOF parallel redundant manipulator is considered to track the following desired path which is presented in cylindrical coordinate:

$$\begin{cases} \upsilon = 0.6t_k \\ \boldsymbol{\gamma}^{\mathrm{d}}(t_k) = 0.2 - (0.2\sin(2.5\upsilon))^2 \\ \mathcal{Z} = (\boldsymbol{\gamma}^{\mathrm{d}}(t_k)\sin(2.5\upsilon))^2 + 1. \end{cases} \tag{28}$$

As seen from Fig. 3, the tracking result of DTNSNP solution (10) in the space rectangular coordinate is relatively precise while NRISP solution (Table I) fails to drive the parallel redundant manipulator to complete the allocated task (28) with constant bias $\Xi(t) = 1$.

Ulteriorly, it can be observed from Fig. 4 that in front of time-dependent linear noise $\boldsymbol{\Xi}(t_k) = t_k + 200$, the steady-state residual errors of DTNSNP solution (10) are 10^{-1}, 10^{-2}, and 10^{-3} as the values of l are set as 0.01 s, 0.001 s, and 0.0001 s, which are at least 10^2 times less than those of NRIP solution, ZDEP solution and ZDTP solution (Table I).

As observed in Fig. 5, with presence of bounded random noise $\Xi(t) \in [499.7, 500.3]$, DTNSNP solution (10) successfully keeps the steady-state residual error less than 0.1. However, the system that programmed by the NRIP solution collapses with the output being 10^3. Though the steady-state residual errors of ZDEP solution and ZDTP solution (Table I) decline as the time sampling interval increases, the corresponding end effector still is not able to work efficiently. Besides, it is rather difficult to infinitely decrease of l.

VI. Conclusions

In this paper, the DTNSN algorithm (8) with the aid of the superior integral control method has been proposed for the manipulator redundancy resolution with the presence of unknown noises. Through thorough analyses and proof, the stability and satisfying convergent performance of the DTNSN algorithm under constant bias, time-dependent noises and bounded random noises have been identified and guaranteed. As a case study, based on the proposed DTNSN algorithm, kinematic solutions have been designed and proposed for serial and parallel redundant manipulators, respectively, which leads to DTNSNS solution and DTNSNP solution with the proven performance. Besides, simulative experiments have substantiated the feasibility of DTNSNS solution and DTNSNP solution. It is noteworthy that with succinct and practical structure, DTNSN algorithm is effective to solve the redundancy resolution with the anti-noise ability, which gives rise to the potential in more industrial applications. Moreover, the research on applying the proposed DTNSN algorithm when the noise is highly complex and solving the requirement that the iterative initial value needs to be close to the theoretical solution would be our future research direction.

References

[1] Z. Xie, L. Jin, X. Du, X. Xiao, H. Li, and S. Li, "On generalized RMP scheme for redundant robot manipulators aided with dynamic neural networks and nonconvex bound constraints," *IEEE Trans. Ind. Inform.*, In press with DOI: 10.1109/TII.2019.2899909.

[2] L. Jin and S. Li, "Distributed task allocation of multiple robots: a control perspective," *IEEE Trans. Syst., Man, Cybern., Syst.*, vol. 48, no. 5, pp. 693–701, May 2018.

[3] R. Cui, C. Yang, Y. Li, and S. Sharma, "Adaptive neural network control of AUVs with control input nonlinearities using reinforcement learning," *IEEE Trans. Syst., Man, Cybern., Syst*., vol. 47, no. 6, pp. 1019–1029, Jun. 2017.

[4] Y. Huang, J. Na, X. Wu, and G. Gao, "Approximation-free control for vehicle active suspensions with hydraulic actuator," *IEEE Trans. Ind. Electron.*, vol. 65, no. 9, pp. 7258–7267, Sep. 2018.

[5] L. Jin, S. Li, H. M. La, X. Zhang, and B. Hu, "Dynamic task allocation in multi-robot coordination for moving target tracking: A distributed approach," *Automatica*, vol. 100, pp. 75–81, 2019.

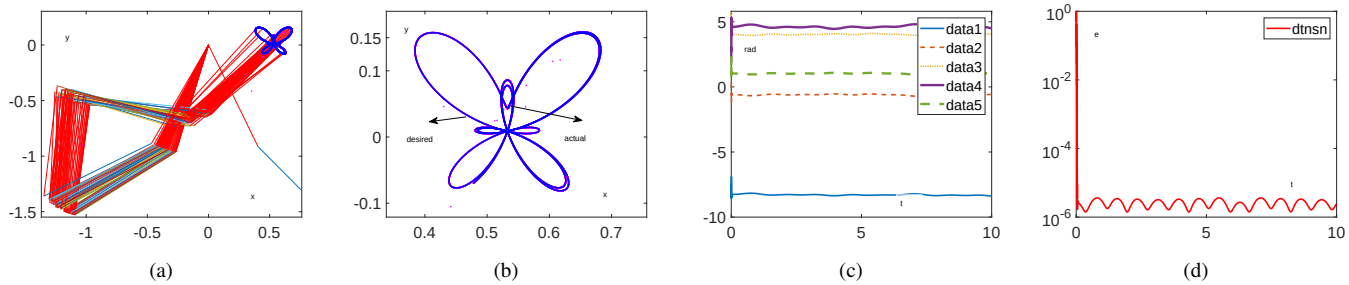

Fig. 1: Profiles of the "butterfly" motion planning (27) on the serial robot manipulator solved by DTNSNS solution (9) with constant bias $\Xi(t) = 2$ and time sampling interval $l = 0.001$ s. (a) Profile of the serial redundant manipulator. (b) Trajectory of the end effector and the desired path. (c) Profiles of joint angle. (d) The steady-state residual error of DTNSNS solution (9).

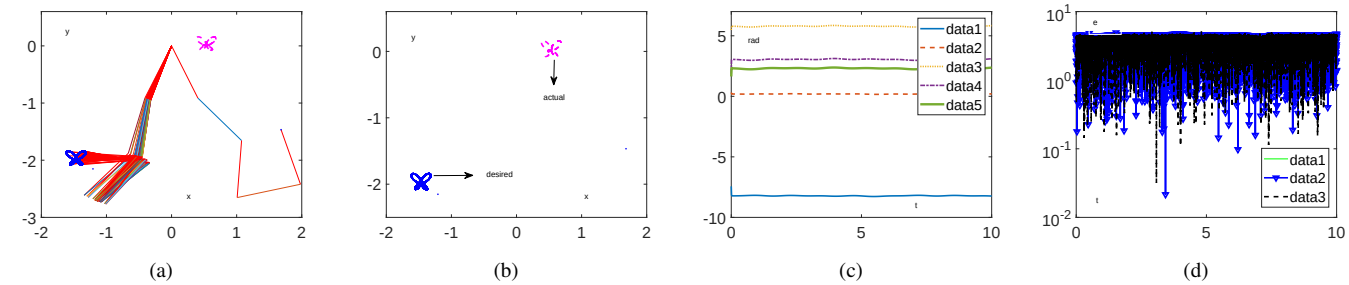

Fig. 2: Profiles of the "butterfly" motion planning (27) on the serial robot manipulator solved by comparable solutions listed in Table I with constant bias $\Xi(t) = 2$ and time sampling interval $l = 0.001$ s. (a) Profile of the serial redundant manipulator synthesized by NRIS solution (Table I). (b) Trajectory of the end effector synthesized by NRIS solution and the desired path. (c) Profiles of joint angle generated by NRIS solution (Table I). (d) Steady-state residual errors of NRIS solution, ZDES solution and ZDTS solution (Table I).

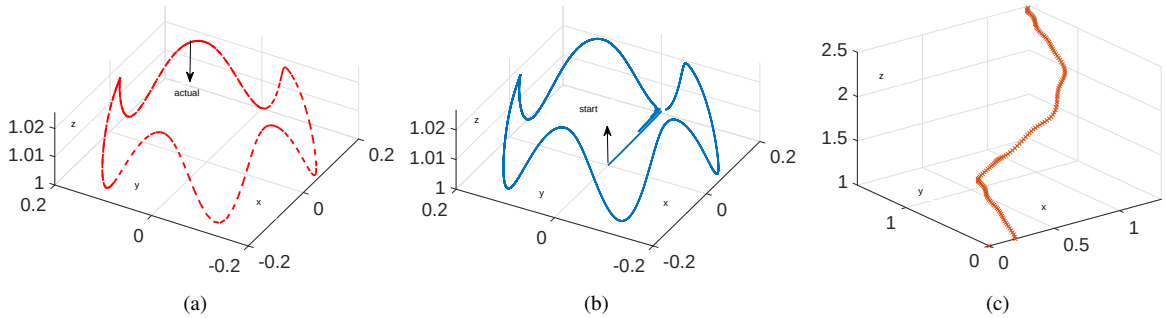

Fig. 3: Comparable simulation results of the motion planning (28) on the parallel robot manipulator with constant bias $\Xi(t) = 1$ and time sampling interval $l = 0.001$ s. (a) Profile of the desired path. (b) Actual trajectory of the end effector generated by DTNSNP solution (10). (c) Trajectory of the end effector generated by NRIP solution (Table I).

[6] L. Jin, S. Li, H. M. La, X. Zhang, and X. Luo, "Manipulability optimization of redundant manipulators using dynamic neural networks," *IEEE Trans. Ind. Electron.*, vol. 64, no. 6, pp. 4710–4720, 2017.

[7] Y. Zhang, S. Li, and X. Zhou, "Recurrent neural network based velocity level redundancy resolution for manipulators subject to joint acceleration limit," *IEEE Trans. Ind. Inform.*, vol. 66, no. 5, pp. 3573–3582, May 2019.

[8] C. A. Klein and C. -H. Huang, "Review of pseudoinverse control for use with kinematically redundant manipulators," *IEEE Trans. Syst., Man, Cybern.*, vol. SMC-13, no. 3, pp. 245–250, Mar. 1983.

[9] B. Liao and W. Liu, "Pseudoinverse-type bi-criteria minimization scheme for redundancy resolution of robot manipulators," *Robotica*, vol. 33, no. 10, pp. 2100–2113, Dec. 2015.

[10] Z. Zhang, A. Beck, and N. Magnenat-Thalmann, "Human-like behavior generation based on head-arms model for robot tracking external targets and body parts," *IEEE Trans. Cybern.*, vol. 45, no. 8, pp. 1390–1400, Aug. 2015.

[11] L. Wei, L. Jin, C. Yang, K. Chen, and W. Li, "New noise-tolerant neural algorithms for future dynamic nonlinear optimization with estimation on hessian matrix inversion," *IEEE Trans. Syst., Man, Cybern.*, In press with DOI: 10.1109/TSMC.2019.2916892

[12] L. Jin, Z. Huang, Y. Li, Z. Sun, H. Li, and J. Zhang, "On modified multi-output Chebyshev-polynomial feed-forward neural network for pattern classification of wine regions," *IEEE Access*, vol. 7, pp. 1973–1980, 2019.

[13] L. Ding, L. Xiao, K. Zhou, Y. Lan, and Y. Zhang, "A new RNN model with a modified nonlinear activation function applied to complex-valued linear equations," *IEEE Access*, vol. 6, pp. 62954–62962, 2018.

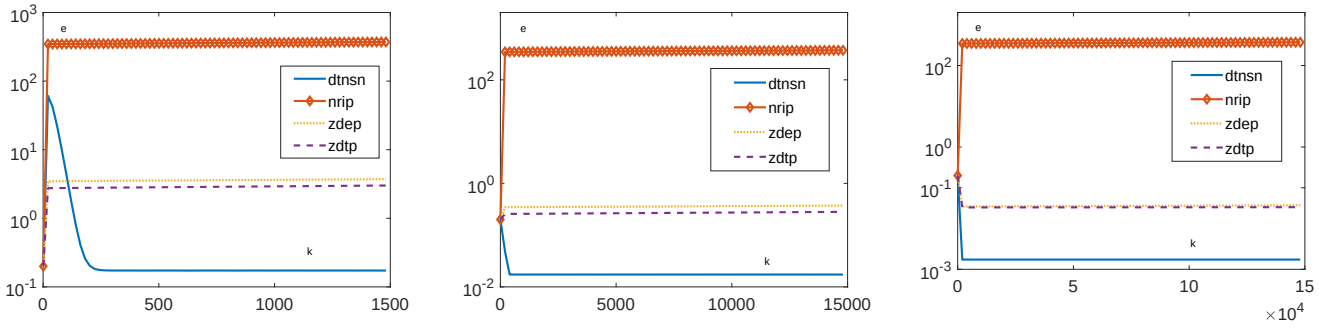

(a) (b) (c)

Fig. 4: Steady-state residual errors of the proposed DTNSNP solution (10), NRIP solution, ZDEP solution and ZDTP solution (Table I) for solving the motion planning (28) with linear noise $\Xi(t) = t_k + 200$. (a) $l = 0.01$ s. (b) $l = 0.001$ s. (c) $l = 0.0001$ s.

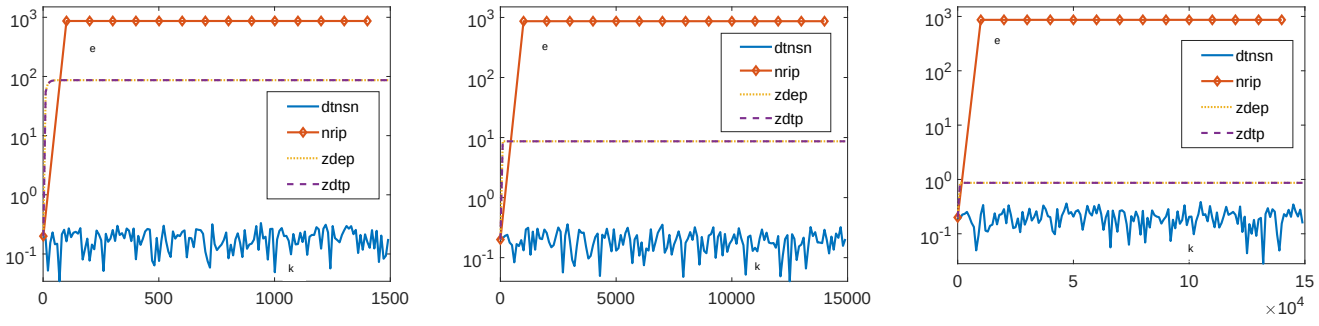

(a) (b) (c)

Fig. 5: Steady-state residual errors of the proposed DTNSNP solution (10), NRIP solution, ZDEP solution and ZDTP solution (Table I) for solving the motion planning (28) with bounded random noise $\Xi(t) \in [499.7, 500.3]$. (a) $l = 0.01$ s. (b) $l = 0.001$ s. (c) $l = 0.0001$ s.

[14] P. S. Stanimirovic, I. Zivkovic, and Y. Wei, "Recurrent Neural Network Approach Based on the Integral Representation of the Drazin Inverse," *Neural Computation*, vol. 27, no. 10, pp. 2107–2131, Oct. 2015.

[15] H. Li, Z. Huang, J. Fu, Y. Li, N. Zeng, J. Zhang, C. Ye, and L. Jin, "Weight and structure determination neural network aided with double pseudoinversion for diagnosis of flat foot," *IEEE Access*, vol. 7, pp. 63146–63154, 2019.

[16] L. Jin, S. Li, X. Luo, Y. Li, and B. Qin, "Neural dynamics for cooperative control of redundant robot manipulators," *IEEE Trans. Ind. Inform.*, vol. 14, no. 9, pp. 3812–3821, Sep. 2018.

[17] H. Lu, L. Jin, X. Luo, B. Liao, D. Guo, and L. Xiao, "RNN for solving perturbed time-varying underdetermined linear system with double bound limits on residual errors and state variables," *IEEE Trans. Ind. Inform.*, In Press with DOI 10.1109/TII.2019.2909142.

[18] L. Chen, Z. Huang, Y. Li, N. Zeng, M. Liu, A. Peng, and L. Jin, "Neural dynamics for cooperative control of redundant robot manipulators," *IEEE Access*, vol. 7, pp. 33001–33008, 2019.

[19] L. Jin, Z. Huang, L. Chen, M. Liu, Y. Li, Y. Chou, and C. Yi, "Modified single-output Chebyshev-polynomial feedforward neural network aided with subset method for classification of breast cancer," *Neurocomputing*, vol. 350, pp. 128–135, 2019.

[20] L. Xiao, S. Li, K. Li, L. Jin, and B. Liao, "Co-design of finite-time convergence and noise suppression: A unified neural model for time varying linear equations with robotic applications," *IEEE Trans. Syst., Man, Cybern., Syst.*, In Press with DOI: 10.1109/TSMC.2018.2870489.

[21] L. Jin, S. Li, B. Hu, M. Liu, and J. Yu, "Noise-suppressing neural algorithm for solving time-varying system of linear equations: A control-based approach," *IEEE Trans. Ind. Inform.*, vol. 15, no. 1, pp. 236–246, Jan. 2019.

[22] A. K. Kaw, E. Kalu, N. Duc, Numerical methods with applications. University of South Florida, 2010.

[23] L. Jin and Y. Zhang, "Discrete-time Zhang neural network for online time-varying nonlinear optimization with application to manipulator motion generation," *IEEE Trans. Neural Netw. Learn. Syst.*, vol. 26, no. 7, pp. 1525–1531, Jul. 2015.

[24] M. W. Spong, S. Hutchinson, and M. Vidyasagar, "Robot Modeling and Control," *New York, NY, USA: Wiley*, 2006.

[25] V. Pan, R. Schreiber, "An improved Newton iteration for the generalized inverse of a matrix with applications," *Journal on Scientific and Statistical Computing*, vol. 12, no. 5, pp. 1109–1130, 1991.

[26] B. M. Wilamowski, N. J. Cotton, O. Kaynak, G. Dundar, "Computing gradient vector and Jacobian matrix in arbitrarily connected neural networks," *IEEE Trans. Ind. Electron.*, vol. 55, no. 10, pp. 3784–3790, 2008.

[27] L. Jin, S. Li, X. Luo, Y. Li, and B. Qin, "Neural dynamics for cooperative control of redundant robot manipulators," *IEEE Trans. Ind. Inform.*, vol. 19, no. 4, pp. 3812–3821, 2018.

[28] B. Liao, Y. Zhang, and L. Jin, "Taylor $O(h^3)$ discretization of ZNN models for solving dynamic equality-constrained quadratic programming with application to manipulators," *IEEE Trans. Neural Netw. Learn. Syst.*, vol. 27, no. 2, pp. 225–237, Feb. 2016.

[29] D. Guo, Z. Nie, L. Yan, "Theoretical analysis, numerical verification and geometrical representation of new three-step DTZD algorithm for time varying nonlinear equations solving," *Neurocomputing*, vol. 214, no. 19, pp. 516–526, 2016.

[30] J. Li, Y. Zhang, S. Li, and M. Mao, "New discretization formula based zeroing dynamics for real-time tracking control of serial and parallel manipulators," *IEEE Trans. Ind. Inform.*, vol. 14, no. 8, pp. 3416–3425, Aug. 2018.

[31] L. Jin, S. Li, B. Liao, and Z. Zhang, "Zeroing neural networks: A survey," *Neurocomputing*, vol. 267, no. 6, pp. 597–604, 2017.

[32] D. Guo, Z. Nie, and L. Yan, "Novel discrete-time Zhang neural network

for time-varying matrix inversion," *IEEE Trans. Syst., Man, Cybern., Syst.*, vol. 47, no. 8, pp. 2301–2310, 2017.

[33] Y. Zhang, L. Jin, D. Guo, Y. Yin, and Y. Chou, "Taylor-type 1-step-ahead numerical differentiation rule for first-order derivative approximation and ZNN discretization," *J. Comput. Appl. Math.*, vol. 273, no. 1, pp. 29–40, 2015.

Xiuchun Xiao received the Ph.D. degree in Communication and Information System in 2013 from Sun Yat-sen University, Guangzhou, China. He is currently an Associate Professor with Guangdong Ocean University. His current research interests include artificial neural network and computer vision.

Lin Wei received the B.E. degree in electrical engineering and information from the Beijing Institute of Technology, Beijing, China, in 2018. She is currently pursuing her M.E. degree in communication and information systems with School of Information Science and Engineering, Lanzhou University, Lanzhou, China. Her research interests include neural networks and robotics.

Dongyang Fu received the Ph.D. degree from the South China Sea Institute of Oceanology, Chinese Academy of Sciences, and the Ph.D. degree from the State Key Laboratory of Satellite Ocean Environment Dynamics, Second Institute of Oceanography, State Oceanic Administration, Guangzhou, China. He is currently a Professor with the School of Electronics and Information Engineering, Guangdong Ocean University, Zhanjiang, China. His current research interests include ocean color remote sensing and its application, remote sensing in offshore water quality, response of upper ocean to typhoon, and neural networks.

Jingwen Yan is a professor at the Department of Electronic Engineering, University of Shantou, China. He is also the associate director of Key laboratory of Digital Signal and Image Processing of Guangdong Province, China. He received his PhD in optics from State Key Laboratory of Applied Optics, Changchun institute of fine mechanics and optics, Academia Sinica in 1997. Since September 2006, he has been working at the Department of Electronic Engineering, University of Shantou, China. His current research is focused on SAR image processing, hyper-wavelet transforms and compressed sensing.

Huan Wang received the B.E. degree from ShanDong JiaoTong University, Jinan, China, in 2018. She is currently pursuing his M.E. degree in physical oceanography at School of Oceanography and Meteorology, Guangdong Ocean University, Zhanjiang, China. Her current research interests include steady state control of the ship, neural networks and ocean color remote sensing.